RESOLVING MULTIMODAL ANGULAR MEASUREMENTS IN COHERENT RADAR NETWORKS USING BAYESIAN ESTIMATION

Isabel Schlangen(1) **and Martin Käske**(2)

(1)*Fraunhofer FKIE, Wachtberg, Germany, Email: isabel.schlangen@fkie.fraunhofer.de*
(2)*Fraunhofer FHR, Wachtberg, Germany, Email: martin.kaeske@fhr.fraunhofer.de*

ABSTRACT

Determining the location of objects in Low-Earth Orbit (LEO) with earthbound sensors is a challenging task due to the large distance of the targets to the Earth's surface. To this end, radar systems are an important modality since they are not restricted by weather conditions and, depending on the architecture, can measure objects at very high ranges. Networks of radars can be used to enhance the localisation accuracy but their architecture implies a multimodal error distribution of the Direction of Arrival (DoA), which might lead to ambiguous measurements in case of low Signal-to-Noise Ratio (SNR) values. This paper provides theoretical considerations about local coherent radar networks, studying the multimodal nature of the corresponding sensor models. Furthermore, it proposes a tracking-based localisation method that integrates the received information over time, hence mitigating the influence of measurements that stem from the secondary modes of the DoA distribution. It is shown in simulation that the proposed tracking approach is able to provide a significant increase in localisation accuracy in comparison to a monostatic setup, even if the number of measurements is low.These preliminary results demonstrate the high potential of using local coherent radar networks for space situational awareness tasks.

Keywords: coherent radar networks, angle estimation, multimodal measurement model, mixture of Gaussians.

1. INTRODUCTION

One of the most important modalities for the observation and cataloguing of space debris is radar technology. From a radar perspective, space debris observation is particularly challenging due to the long distances between the objects of interest and the observer on the one hand and the small size of many objects on the other.

One method to increase the performance of a space debris sensing system is to use a network of radars in a multistatic setup [1]. Local coherent radar networks, whose nodes are typically not further than a few hundred metres apart, show a quasi-monostatic behaviour since the distance between the nodes is negligibly small compared to the distance to the observed objects in Low-Earth Orbit (LEO). Thus, we model the antennas of a coherent local network as one big antenna array. However, if each node of the network is equipped with an antenna array, the joint array will become sparse. The elements of each individual array are usually densely spaced, i.e. neighbouring elements are less than half a wavelength apart, exhibiting low sidelobes in their spatial/angular response allowing for estimates free of ambiguities. Elements of different subarrays in the joint sparse array are much further apart, which leads to high sidelobes in the joint response. In particular, the estimated Direction of Arrival (DoA) is distributed according to a network-specific function that depends on the antenna architecture as well as the relative location of the nodes. Usually, the DoA estimation error is assumed to be Gaussian distributed within a single mode around the true value. In a sparse array, this distribution becomes multi-modal, with the highest peak centred on the true DoA of the object surrounded by several side lobes with significant amplitude, whose number and location depend on the configuration of the network. The effect of high sidelobes or grating lobes in sparse arrays has been reported in the past [2]. Strategies to mitigate the problem encompass the simultaneous use of multiple carriers at sufficiently different wavelengths such that the grating lobes are reduced [3].

Not considering the multi-modal nature of the error can have a significant impact on the evaluation of estimation results as well as any subsequent data processing such as tracking to improve the estimates. The occurrence of multi-modal errors is not limited to angular estimates in coherent networks but always occurs when sampling, performed in some domain, exhibits gaps or pauses. This is discussed and illustrated for example in [4] for the estimation of radial velocities or Doppler shifts in pulsed radars with sufficiently large duty cycles (ration between pulse length and Pulse Repetition Interval (PRI)).

This paper first gives theoretical considerations about the multi-modality of angular measurements obtained by local radar networks (Sec. 2) and then proposes to use a Bayesian approach to process the described multi-modal DoA estimates over time (Sec. 3). Instead of trying to reduce the level of the sidelobes, their effect is incorporated into the signal processing scheme. In particular, the sensor model is approximated as a mixture of Gaussians corresponding to the underlying probability distribution stemming from the architecture of the considered radar network. In the filtering recursion, the current state is first predicted according to a suitable motion model (e.g. Kepler dynamics or a local near-constant velocity approximation) and then corrected with the incoming measurement using the characteristic sensor model of the network. This procedure is applied in simulation to different examples of network configurations as a proof of concept, including a monostatic baseline case, a triangular network with three nodes, and a cross-shaped network with five nodes. The simulations in Sec. 4 show that the applied filtering is effective in resolving the modes, resulting in a DoA error that is closer to a single Gaussian distribution. The improved DoA accuracy due to the increased aperture size of the coherent network is retained, resulting in a smaller error covariance of a tracked target in comparison to the monostatic scenario.

2. ANGULAR ESTIMATION USING LOCAL RADAR NETWORKS

2.1. Problem description

In general, the estimation of the DoA is a two-dimensional problem, i.e. the estimation of the azimuth and elevation angles or u and v coordinates of an incoming (or emitted) planar electromagnetic wave. An antenna array receives the signal of the wave and creates spatial samples at each of the elements of the array. The estimation problem has a unique solution if each DoA corresponds to exactly one pattern of sampling values. If such a mapping exists, the direction can be derived from the received pattern in a unique manner. Ambiguities, on the other hand, occur if multiple DoAs lead to the same sampling pattern and hence cannot be distinguished. To avoid such effects, conditions on the configuration of the array can be formulated, e.g. a distance of less than half of the incoming wavelength between two neighbouring elements (Nyquist-Shannon sampling theorem).

In a local coherent radar network, one can interpret the entirety of all individual elements of each network node as one big array, which is sparse due to the distances between the different nodes. Like this, the DoA of an object can be estimated not only at each individual node but by the network antenna as a whole. Due to the distances between the nodes, the sampling condition is violated globally, however not at the individual arrays.

Another important factor that influences the performance of the DoA estimation is that radar systems, as indeed all sensors, are subject to noise stemming from the underlying physical properties of the system. Additional noise distorts the actual sampling pattern, which may lead to wrong estimates or create ambiguities artificially. The influence of this effect depends on the intensity of the noise (in terms of the Signal-to-Noise Ratio (SNR)) as well as the cost function of the maximum-likelihood estimator.

2.2. An illustrative example

To illustrate the problem described in Sec. 2.1, let us consider a periodic time domain signal in terms of a complex phasor with unknown complex amplitude γ and frequency f_0:

$$u\left(t; f_0\right) = \gamma e^{j2\pi f_0 t} \tag{1}$$

$$\left|f_0\right| < \frac{f_p}{2} \tag{2}$$

The goal is to estimate the frequency of the signal based on sampling which is influenced by additive white noise. Samples are drawn equidistantly in a limited observation window of length T_h, as shown in Fig. 1 with a sampling rate f_p. It is further assumed that the Shannon-Nyquist

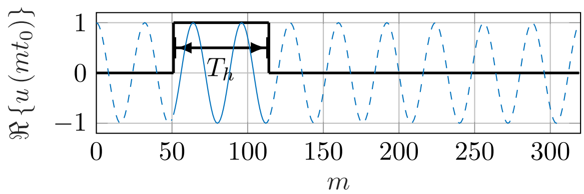

Figure 1: Sinusoid signal with limited observation window.

sampling theorem holds, i.e. ambiguities due to aliasing are excluded. The windowed signal can be represented by

$$u\left(t; f_0\right) \cdot h\left(t - t_a\right) = \gamma s\left(t; f_0\right). \tag{3}$$

The window function $h\left(t - t_a\right)$ is rectangular with a duration of T_h, starting at $t = t_a$. A given sampling rate $t_0 = 1/f_p$ results in a predetermined number of sampling points that are collected in a vector $\mathbf{s}$. Furthermore, complex white noise with given variance σ_n^2 is added, leading to

$$\mathbf{x} = \mathbf{s}\left(f_0\right) + \mathbf{n} \in \mathbb{C}^{M\times 1}, \tag{4}$$

$$\mathbf{n} \propto \mathcal{CN}\left(0, \mathbf{R}_n = \sigma_n^2 \mathbf{I}\right). \tag{5}$$

To determine the frequency, a cost function based on a scaled negative log-likelihood function is defined and maximised:

$$l\left(x; \gamma, f\right) = \left(\mathbf{x} - \gamma \mathbf{s}\left(f\right)\right)^H \mathbf{R}_n^{-1} \left(\mathbf{x} - \gamma \mathbf{s}\left(f\right)\right). \tag{6}$$

Since only the frequency is of interest and γ is a linear parameter, it is possible to modify (6) according to the considerations in [6], replacing γ by its estimate $\widehat{\gamma} = \left[\mathbf{s}\left(f\right)^H \mathbf{R}_n^{-1} \mathbf{s}\left(f\right)\right]^{-1} \mathbf{s}\left(f\right)^H \mathbf{R}_n^{-1} \mathbf{x}$:

$$\mathcal{L}\left(x; f\right) = \mathbf{x}^H \mathbf{R}_n^{-1} \mathbf{s}(f) \left[\mathbf{s}(f)^H \mathbf{R}_n^{-1} \mathbf{s}(f)\right]^{-1} \mathbf{s}(f)^H \mathbf{R}_n^{-1} \mathbf{x}, \tag{7}$$

$$\widehat{f} = \max_f \mathcal{L}\left(x; f\right). \tag{8}$$

In case the covariance matrix of the additional noise is a scaled identity matrix, the problem can be further simplified to

$$\widehat{f} = \max_{f} \frac{1}{|\mathbf{s}(f)|^2} \left| \mathbf{s}(f)^H \mathbf{x} \right|^2 . \tag{9}$$

In order to solve (9), the cost function can be determined on any grid of frequencies by maximising over all samples. A special case is the grid $f = k\frac{1}{T_h}; k = [0, \ldots, M-1]$ in combination with a rectangular window function, since the term $|\mathbf{s}(f)|^2$ is constant in this case. This case corresponds to the DFT of the signal. Figure 2 shows the cost function for an example without noise. Here, the desired frequency f_0 lies on one of the sampling points of the DFT. This example shows that, except for the actual frequency f_0, all DFT sampling values are close to zero. If another grid was used, the secondary maxima of the window function would cause higher returns. Additional noise would further distort the cost function and cause the global maximum to shift from f_0 to another frequency. The difference between the estimated and the true frequency hence depends on the SNR and the shape of the cost function. According to maximum-likelihood theory, the error can be modelled asymptotically Gaussian, i.e. the deviation is approximally Gaussian distributed for high enough SNR [6].

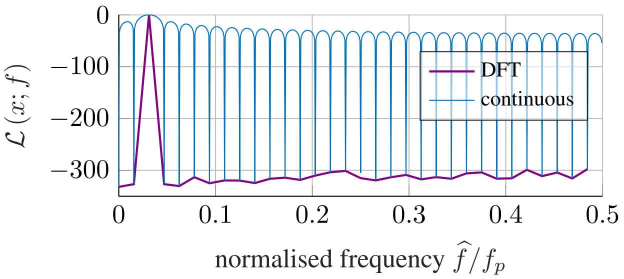

Figure 2: Continuous spectrum with DFT as a special sampling grid.

It is further possible to expand the signal observation to multiple windows that can be located in any configuration. An example with two observation windows is shown in Figure 3, where the gap between them is exactly one window length ($T_g = T_h$). This setup corresponds to the DoA estimation in a local radar network with two nodes, the two antenna arrays being situated exactly one array width apart. The resulting cost function (without noise) results in the red pattern shown in Figure 4. Note that the blue curve in Fig. 4 corresponds to the single-window signal in Fig. 2, whereas the green curve represents a constellation with four concatenated windows (i.e. without gaps). It can be seen that the main lobe is significantly narrower if more than one window is used. The first side lobe, however, is considerably stronger and closer to the maximum of the cost function. If instead, a large window with four times the width of the window size T_h without gaps was used instead (see the green curve in Fig. 4), this would result both in a narrow main lobe and weak side lobes at the same time.

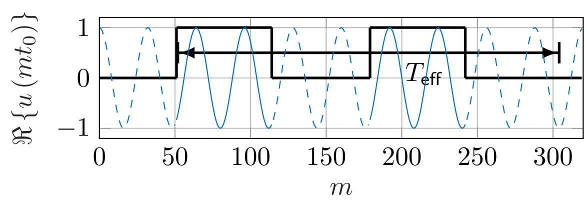

Figure 3: Sinusoid signal with two observation windows.

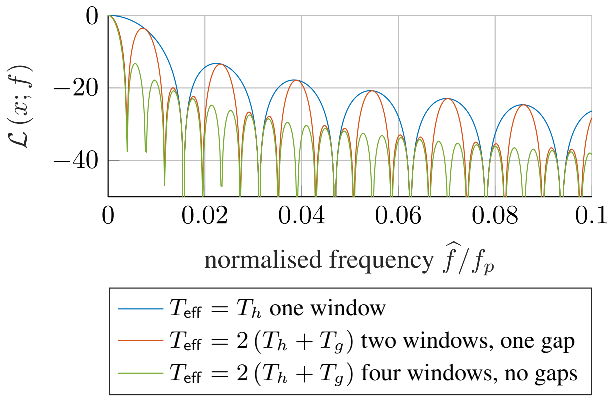

Figure 4: Cost function for observations with different duration/gaps.

Hence it can be concluded that the width of the main lobe is dependent on the effective observation time T_{eff}, i.e. the main lobe is as narrow as in the case of a big window of length T_{eff} but without gaps. The envelope of the side lobes still follows the curve for a single window in this case. The width of the main lobe further decreases if the gaps between the windows are increased, however the secondary maxima increase as well and move closer to the main lobe. This effect, in combination with critically low SNR, increases the risk of shifting the estimate to one of the side lobes, which is less likely in a single-window scenario. Still, the lobes are well-separated by gaps caused by the roots of the cost function.

To visualise the estimation error with different gap lengths, a simple Monte Carlo experiment was conducted. The histogram of the estimation error is shown in Fig. 5. The figure demonstrates that the gaps result in a multi-modal estimation error. Furthermore, longer gap lengths lead to a more narrow centre peak, but also to a higher number of estimations in secondary maxima. Note that the estimator is always unbiased independent of the gap size, i.e. the expected value over all realisations always coincides with the true value. Thus, it appears useful to model the error distribution with a mixture of Gaussians instead of a single Gaussian distribution since each mode of the error function appears to be Gaussian distributed.

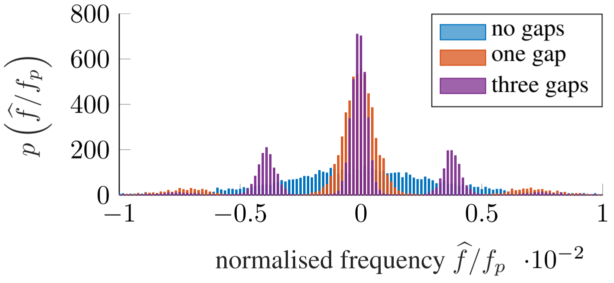

Figure 5: Histogram of the estimation error using different window sizes. SNR $= 9\,\text{dB}$, $N_{\text{mc}} = 10000$.

3. GAUSSIAN-MIXTURE APPROXIMATION OF MULTI-MODAL DOA MEASUREMENTS

As seen in the previous section, measuring the DoA can be seen as a random experiment based on a multimodal distribution which can in general be approximated with a Gaussian mixture density. The random nature of the problem implies that one measurement is not sufficient to exclude samples from side lobes, therefore this paper proposes a Bayesian approach which takes the temporal evolution of the measurement into account. For this purpose, let us describe the *hidden state* of the measured object of interest in the uv space, where $x_{k|k} = [u_k, \dot{u}_k, v_k, \dot{v}_k] \in \mathbb{R}^4$ represents the uv position $[u_k, v_k]$ and velocity $[\dot{u}_k, \dot{v}_k]$ at discrete time steps k. A Bayes filter is composed of a prediction and an update step, with which the current state x_{k-1} is first predicted to time k using a transition model $f_{k|k-1}$ and then updated w.r.t. the incoming measurement z_k using the sensor model g_k. In the present case, g_k is a Gaussian Mixture with G components $\mathcal{N}(x^g_{k|k}, P^g_{k|k})$, centred on $x_{k|k}$, where $x^g_{k|k} = x_{k|k} + \Delta_g$ and $P^g_{k|k} \in \mathbb{R}^{4\times4}$ for all $1 \leq g \leq G$. The arrangement of the Gaussians is assumed to be given by the Δ_gs which depend on the network geometry and constant over time. This makes it possible to use the well-known Kalman prediction [5]:

$$x_{k|k-1} = F_k x_{k-1|k-1}, \tag{10a}$$

$$P_{k+1|k} = F_k P_{k-1|k-1} F_k^T + Q_k \tag{10b}$$

where $F_k, Q_k \in \mathbb{R}^4$ are the transition and process noise matrices, respectively. After receiving the new measurement $z_k = [\hat{u}_k, \hat{v}_k, \hat{r}_k]$, the respective innovation y^g_k with covariance S^g_k is computed for each component g of the sensor model:

$$y^g_k = z_k - H_k x^g_{k|k-1}, \tag{11a}$$

$$S^g_k = H_k P_{k|k-1} H_k^T + R_k, \tag{11b}$$

where $H_k \in \mathbb{R}^{2\times4}$ maps the target state x_k into the measurement space and $R_k \in \mathbb{R}^{2\times2}$ denotes the covariance of the additive measurement noise. If the measurement falls into the 3σ gate of component g, i.e. $y^T S^{-1} y < \text{chi2inv}(0.99, 3)$, the Kalman gain K^g_k is computed and to determine the corrected target state as follows:

$$K^g_k = P_{k|k-1} H_k^T S_k^{-1}, \tag{12a}$$

$$x_{k|k} = x_{k|k-1} + K^g_k y^g_k, \tag{12b}$$

$$P^g_{k|k} = (I - K^g_k H_k) P_{k|k-1}. \tag{12c}$$

4. EXPERIMENTS

4.1. Simulated network architectures

The following simulations with one moving target serve to demonstrate the applicability of the filter-based resolution of multi-modal angular measurements. For this purpose, a quasi-monostatic setup as well as two networks with different architectures are tested. The main configurations of the three systems are shown in Fig. 6. To determine the required size and location of the components of the required Gaussian mixture for each network architecture, a simulated static target is used. The Monte Carlo simulation of the resulting measurements for a target with 9 dB SNR is shown in Figure 7 (coloured samples), along with the fitted mixture (black ellipses). In case of the cross configuration, the nine highest-weight components are used, which are allocated in a 3×3 grid with a respective distance of 0.0214 in u and v. The central compo-

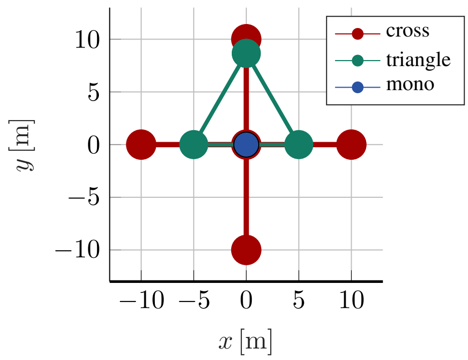

Figure 6: Configuration of receiver nodes in the three tested networks.

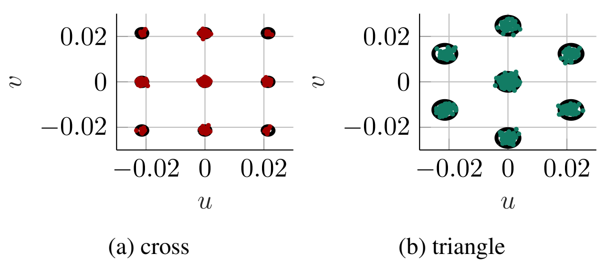

Figure 7: Modes of the DoA estimation for a static target with 9 dB SNR. The black ellipses represent the 3σ covariance gate.

nent is weighted with 0.5294, while the remaining components receive a weight of 0.0588. All covariances are assumed to have the same size, determined as the covariance of the central cluster of estimates. In this example, the covariance is determined to be $\mathrm{cov}(u, u) = 3.7483 \cdot 10^{-7}$, $\mathrm{cov}(v, v) = 3.7763 \cdot 10^{-7}$ with off-diagonal terms $\mathrm{cov}(u, v) = \mathrm{cov}(v, u) = -9.8651 \cdot 10^{-10}$.

The distribution function of the triangle configuration also exhibits a central component, which receives a weight of 0.5385. Due to the triangular allocation of the nodes, only six side lobes manifest in the resulting distribution, as seen in Figure 7b, which receive equal weights of 0.0769. These side lobes form a hexagonal pattern around the central lobe with a respective distance of 0.0247 to it. The resulting covariance of the components is four times bigger than that of the cross-shaped network since the same u/v area is described by fewer components in comparison.

The third setup of comparison is a monostatic sensor with (approximate) unimodal error distribution. This distribution, however, needs a 230-fold bigger covariance in comparison to the triangle configuration described above. Furthermore, the velocity covariance of each configuration is set to $\mathrm{cov}(\dot{u}, \dot{u}) = \mathrm{cov}(\dot{v}, \dot{v}) = 10^{-2}$ and $\mathrm{cov}(\dot{r}, \dot{r}) = 10.0$, respectively. Please note, that for sufficiently low SNR also the monostatic sensor would exhibit multiple modes as any practical likelihood function (with finite measurement aperture) posses sidelobes although they might be weak.

Note that alongside the angle, range measurements can also be taken into account. However, the range error distribution is unimodal, hence it is not shown in the experiments presented below. If Doppler measurements are considered, multi-modality is in fact expected along the Doppler dimension if a pulsed radar (with appropriate duty cycle) is used. This case is presented in [4].

Note that the measurement function needs to be tailored to the specific network architecture, i.e. a mixture with suitable means and covariance matrices needs to be found. In case an analytic solution cannot be found, it is possible to use an expectation-maximisation approach to optimise the mixture [8].

4.2. Initialisation of the tracker

Further assumptions need to be formulated to initialise the tracking algorithm. The initial state estimate is centred on the position of the initial DoA measurement with 0 velocity in u and v, i.e. $x_{0|0} = [\hat{u}_0, 0, \hat{v}_0, 0]$. In the following experiments, the orbit is approximated with a Near-Constant Velocity (NCV) model with transition matrix $F_k = \mathcal{I}_2 \otimes \begin{pmatrix} 1 & T \\ 0 & 1 \end{pmatrix}$ (cf. (10)). The standard deviation of the acceleration noise is set to $\sigma_{\mathrm{acc}} = 10^{-5}$, while the standard deviation of the measurement noise is chosen to be $\sigma_{u/v} = 0.001$. Both the target state as well as the measurements are handled in u/v space, i.e. the measurement matrix has the form $H_k = \begin{pmatrix} 1 & 0 & 0 & 0 \\ 0 & 0 & 1 & 0 \end{pmatrix}$.

4.3. Results

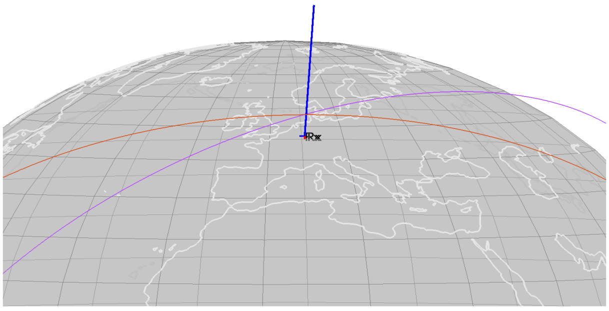

Figure 8: Illustration of the quasi-monostatic setup with two possible target orbits.

As described before, the following experiments are concerned with a single moving target as shown exemplarily in Figure 8. The receiver nodes are placed according to the configurations in Figure 6 and a Kepler orbit is simulated that traverses the zenith of the central receiver. The total observation length is restricted to $10\,\mathrm{s}$, leading to the angular positions shown in Figure 9.

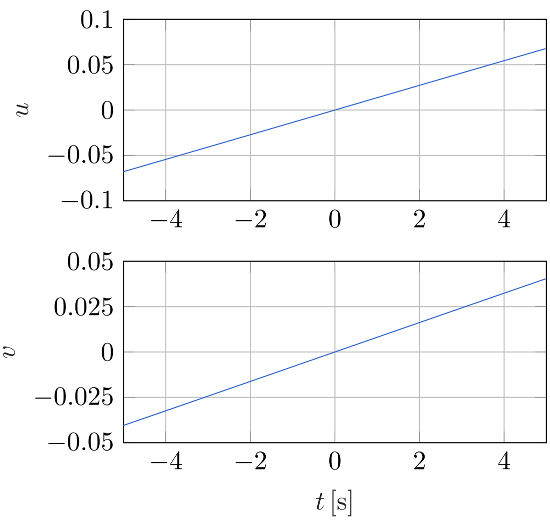

Figure 9: Simulated angular position of an example orbit in u and v coordinates over time.

An important parameter for the simulation is the time delta between the measurements. In this paper, the two cases $\Delta t = 23.3\mathrm{ms}$ and $\Delta t = 233\mathrm{ms}$ are considered. The choice of these values is based on the assumption that the target is located at a maximum distance of $3500\,\mathrm{km}$ from the radar, resulting in a PRI of $2r_{max}/c_0 \approx 23.3\,\mathrm{ms}$. The other Δt value, on the other hand, assumes a Coherent Processing Interval (CPI) over ten pulses. For the simulations, noisy measurements are generated from the ground truth assuming a given SNR and the angles are determined iteratively with a maximum-likelihood estimator.

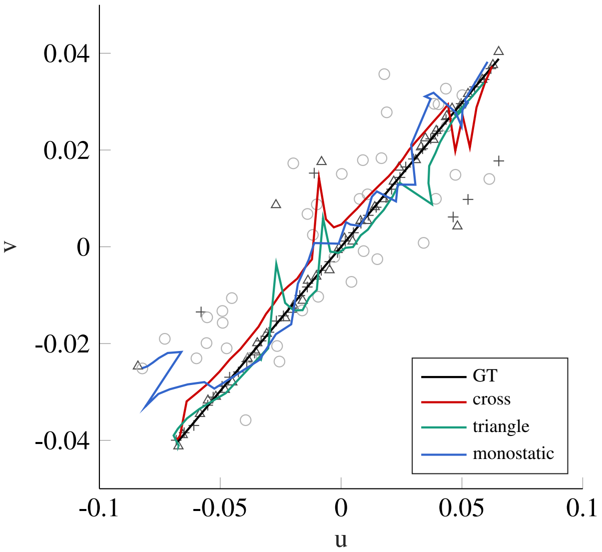

Figure 10: Estimated trajectories, SNR 14 dB, $\Delta t = 233\,\text{ms}$. Measurements of the cross, triangle and monostatic setups are marked as $+$, $\triangle$ and $\circ$, respectively.

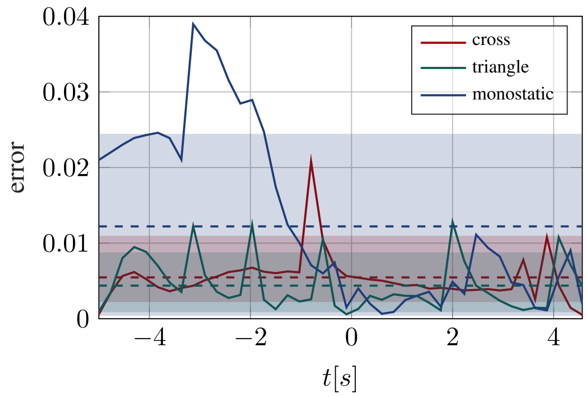

Figure 11: Angle error $||[\hat{u}; \hat{v}] - [u_{\mathsf{GT}}; v_{\mathsf{GT}}]||_F$ with temporal mean and variance for the three configurations, SNR 14 dB, $\Delta t = 233\,\text{ms}$.

Figure 10 displays the results for the different network configurations as shown in Figure 6, assuming an SNR of 14 dB and an assumed coherent integration over 10 pulses. The true values are depicted in black, the filtered results in red, green, and blue and the corresponding measurements as $+$, Δ and $\circ$ symbols, respectively. The reason for the choice of a relatively high SNR is that in reality, the monostatic benchmark case also has a multimodal nature, however for higher SNR values $> 10\,\text{dB}$ the distribution is sufficiently approximated by a unimodal Gaussian [6].

In Figure 10 it can be seen that because of the high SNR, the vast majority of detections originate from the central mode in all configurations. Since the monostatic case has a much wider central mode than the networks, its angle estimations ($\circ$) are much less accurate than in the cross ($+$) and triangle ($\triangle$) configurations. On the other hand, a few estimates of the networks originate from secondary modes. The estimated trajectories (Figure 10, coloured lines) and the corresponding error plots (see Figure 11) reflect this behaviour: If the tracker uses angular measurements from one of the network configurations, the trajectories follow the ground truth much more closely, however a measurement from a side lobe results in a sharp increase in error. The monostatic measurements, on the other hand, have no side lobes but still lead to a much higher estimation error overall. The error can

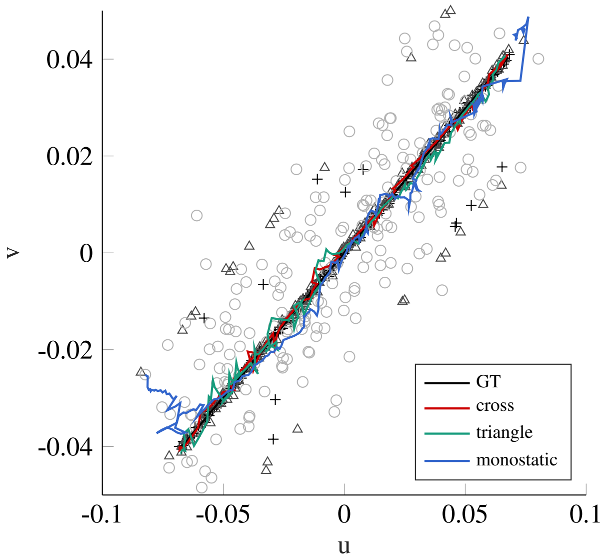

Figure 12: Estimated trajectories, SNR 14 dB, $\Delta t = 23.3\,\text{ms}$. Measurements of the cross, triangle and monostatic setups are marked as $+$, $\triangle$ and $\circ$, respectively.

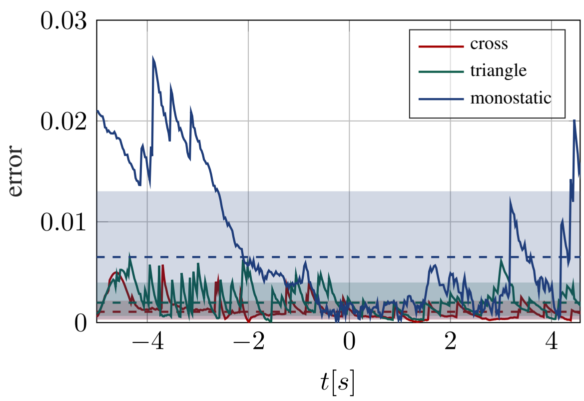

Figure 13: Angle error $||[\hat{u}; \hat{v}] - [u_{\mathsf{GT}}; v_{\mathsf{GT}}]||_F$ with temporal mean and variance for the three configurations, SNR 14 dB, $\Delta t = 23.3\,\text{ms}$.

be reduced even further with smaller time intervals of 23.3 ms, as shown in Figure 12 and Figure 13. While the cross and triangle network configurations receive more estimates from secondary modes as seen in Figure 12, the resulting tracks are much more stable since more information is available overall. It can be observed that the cross configuration is the most accurate in this case since it has the highest amount of information available. The monostatic case, however, still needs to compensate for the wide main lobe, causing a much higher error.

In both presented cases it can be noted that the tracker using monostatic measurements needs much more time to converge and hence the average error (dashed line) and its variance (shaded area) is much higher than for the multistatic cases. It can be concluded that the combination of using a multistatic framework with a tracking approach leads to a faster and more accurate target localisation. While short PRIs are beneficial for high accuracies, longer coherent processing intervals can still be used to save resources for other tasks, given that the average error of the monostatic case with $\Delta t = 23.3\,\mathrm{ms}$ still has a higher error (0.013 radians) than the networks with $\Delta t = 233\,\mathrm{ms}$ (0.010 and $0.009\,\mathrm{rad}$, respectively).

5. CONCLUSION

This paper presented a method to process multimodal angular measurements that result from using local coherent radar networks for orbit determination and tracking objects in LEO. A simple example was given to explain how multimodal measurements result in ambiguities if a multistatic radar system is subject to high levels of noise. Then, a Gaussian mixture approach was presented that models the sensor in terms of a sum of Gaussian distributions. This mixture represents the error distribution in the received DoA values, which is dependent on the array architecture as well as the network configuration. To analyse the proposed tracking approach, a simple scenario was created, measuring an object travelling over the zenith of a radar network. Two architectures, namely a cross-shaped setup with five nodes and a triangular setup with three nodes, were simulated and compared with a monostatic setup. The provided results showed that using a local radar network brings much higher localisation accuracies even in the presence of measurements coming from a multimodal sensor model. It is even possible to obtain lower errors with local networks with a coherent processing interval of ten pulses in comparison with using each pulse of the corresponding monostatic setup. This effect stems from the much smaller principal mode of the error distribution, which even compensates for the spontaneously occurring measurements from secondary modes. An important aspect is the temporal integration achieved by the Bayesian approach, which is able to mitigate the side lobe measurements.

ACKNOWLEDGEMENTS

The project on which this report is based was funded by the German Federal Ministry for Economic Affairs and Climate Action under the funding code 50 LZ 2005. Responsibility for the content of this publication lies with the author.

REFERENCES

1. Javadi, S. H., & Farina, A. (2020). Radar networks: A review of features and challenges. *Information fusion*, 61, 48-55.
2. F. Athley, C. Engdahl & P. Sunnergren (2007). On radar detection and direction finding using sparse arrays *IEEE Transactions on Aerospace and Electronic Systems, vol. 43, no. 4, pp. 1319-1333, October 2007*
3. S. Zhou, Y. Fang & D. Wu (2022), Improvement method of low-altitude angle measurement ambiguity of array radar *4th International Conference on Communications, Information System and Computer Engineering (CISCE)*
4. Kollecker, S., & Horstmann, S. (2025). Radial Velocity Ambiguity Resolution for the Pulsed Space Surveillance Radar GESTRA. *Submitted and Accepted to 9th European Conference on Space Debris*.
5. Kalman, R. E. (March 1, 1960). A New Approach to Linear Filtering and Prediction Problems. *ASME. J. Basic Eng.*, 82(1), 35–45.
6. Kay, S. M. (1993). *Fundamentals of statistical processing, volume I: Estimation theory*.
7. Skolnik, M. I. (1980). *Introduction to radar systems*. New York: McGraw-Hill.
8. Vlassis, N., & Likas, A. (2002). A greedy EM algorithm for Gaussian mixture learning. *Neural processing letters*, 15, 77-87.